Identification of the Protein Binding Region of *S*-Trityl-L-cysteine, a New Potent Inhibitor of the Mitotic Kinesin Eg5[†]

Sébastien Brier,[‡] David Lemaire,[‡] Salvatore DeBonis,[§] Eric Forest,*[,‡] and Frank Kozielski*[,§]

Laboratoire de Spectrométrie de Masse des Protéines (LSMP) and Laboratoire de Microscopie Electronique Structurale (LMES), Institut de Biologie Structurale (CEA-CNRS-UJF), 41, rue Jules Horowitz, 38027 Grenoble Cedex 01, France

Received April 14, 2004; Revised Manuscript Received July 15, 2004

ABSTRACT: Human Eg5, a mitotic motor of the kinesin superfamily, is involved in the formation and maintenance of the mitotic spindle. The recent discovery of small molecules that inhibit HsEg5 by binding to its catalytic motor domain leading to mitotic arrest has attracted more interest in Eg5 as a potential anticancer drug target. We have used hydrogen−deuterium exchange mass spectrometry and directed mutagenesis to identify the secondary structure elements that form the binding sites of new Eg5 inhibitors, in particular for *S*-trityl-L-cysteine, a potent inhibitor of Eg5 activity *in vitro* and in cell-based assays. The binding of this inhibitor modifies the deuterium incorporation rate of eight peptides that define two areas within the motor domain: Tyr125−Glu145 and Ile202−Leu227. Replacement of the Tyr125−Glu145 region with the equivalent region in the *Neurospora crassa* conventional kinesin heavy chain prevents the inhibition of the Eg5 ATPase activity by *S*-trityl-L-cysteine. We show here that *S*-trityl-L-cysteine and monastrol both bind to the same region on Eg5 by induced fit in a pocket formed by helix α3−strand β5 and loop L5−helix α2, and both inhibitors trigger similar local conformational changes within the interaction site. It is likely that *S*-trityl-L-cysteine and monastrol inhibit HsEg5 by a similar mechanism. The common inhibitor binding region appears to represent a "hot spot" for HsEg5 that could be exploited for further inhibitor screening.

The mitotic spindle plays a crucial role in cell division and is thus an important target in cancer chemotherapy. Antimitotic tubulin agents, such as the vinca alkaloids and the taxanes, interfere with the polymerization−depolymerization process of microtubules leading to cell cycle arrest in mitosis (*1*). However, these microtubule poisons display several undesirable side effects, such as neurotoxicity, due to the disruption of tubulin function in nondividing cells (*2*). In addition, resistance to the current tubulin-binding drugs during prolonged treatments has also been reported (*3*). Consequently, there is clearly a need to explore alternative approaches to achieve mitotic spindle inhibition. Although several strategies have been proposed for the development of less toxic tubulin poisons, an interesting alternative is to target proteins that are directly involved in cell division such as the check point proteins or the mitotic kinesins (*1*). Many of these proteins are very specialized and are only active at specific phases of the cell cycle. We might thus expect that their inhibition will produce fewer side effects in nondividing cells than the current tubulin drugs have produced.

The BimC members of the kinesin superfamily are involved in mitotic spindle dynamics in a wide variety of organisms (*4*, *5*). The human member of this subfamily (called Eg5 throughout the text) is essential for the formation of the bipolar spindle *in vivo*. Eg5 is required for centrosome separation during prophase/prometaphase (*6*). The localization of Eg5 during the cell cycle is complex and depends on the phosphorylation state of a short 40-amino acid stretch in the tail domain termed the BimC box (*6*, *7*). This box is highly conserved within the BimC family and contains a potential $p34^{cdc2}$ phosphorylation site (*8*). The inhibition of Eg5 function by microinjection of antibodies against the C-terminal tail domain blocks centrosome migration and causes HeLa cells to arrest in mitosis with a characteristic monoastral spindle comprised of a radial array of microtubules surrounded by a ring of chromosomes (*6*). This inhibition only occurs before the metaphase stage. Eg5 thus appears as a potential protein target for antimitotic drugs (*9*). The first small molecule inhibitor of Eg5, named monastrol, was identified using a phenotype-based screen (*10*). This cell permeable compound blocks mitosis in *Xenopus laevis* by binding reversibly to Eg5 without further effect through the S and G2 phases of the cell cycle (*11*). As a result, cells arrest midway through mitosis with monoastral spindles. Recent studies have shown that the minimal monastrol binding domain in Eg5 is located within the motor domain (*12*, *13*). In addition, several novel classes of molecules such as terpendole E (isolated from a fungal strain) and quinazolinones have recently been identified as inhibitors of Eg5 function (*14*, *15*). One of these quinazolinone analogues

[†] This work has been funded by grants from ARECA (Alliance des Recherches sur le Cancer), ARC (Association pour la Recherche sur le Cancer, Contract 5197), and the Rhône-Alpes region (Contracts 03 013690 02 and 03 013690 01). S.B. is supported by a Ph.D. grant from the CNRS (Centre National de la Recherche Scientifique).

* To whom correspondence should be addressed. F.K.: telephone, 0033-4-3878-4024; fax, 0033-4-3878-5494; e-mail, Frank.Kozielski@ibs.fr. E.F.: telephone, 0033-4-3878-3403; fax, 0033-4-3878-5494; e-mail, Eric.Forest@ibs.fr.

[‡] Laboratoire de Spectrométrie de Masse des Protéines (LSMP).

[§] Laboratoire de Microscopie Electronique Structurale (LMES).

10.1021/bi049264e CCC: $27.50
Published on Web 09/25/2004

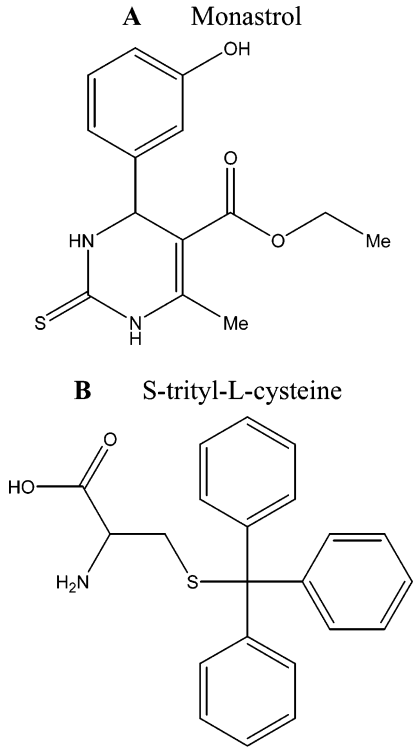

FIGURE 1: Chemical structures of the Eg5 inhibitors (A) monastrol and (B) *S*-trityl-L-cysteine.

appears to have a broad spectrum activity against murine and human solid tumor models.

Here we use hydrogen−deuterium (H/D)[1] exchange experiments associated with protein digestion and mass spectrometry (*16*, *17*) and directed mutagenesis for the identification of the binding region of different inhibitors targeting Eg5. The rate at which hydrogens located at peptide amide linkages undergo isotopic exchange is highly dependent on their environment and depends on whether the hydrogens are participating in intramolecular hydrogen bonding as well as on the extent to which the hydrogens are shielded from the solvent (*18*). In addition, the binding of ligands to a protein may also affect amide hydrogen exchange (*19*). Therefore, analysis of the H/D exchange rate represents a sensitive tool for studying protein structure and dynamics as well as protein surfaces involved in inhibitor binding. H/D exchange in association with mass spectrometry has been extensively used to characterize the tertiary structure of proteins (*17*, *20*−*22*) and conformational changes upon ligand binding (*23*−*26*).

We first validated our approach using the Eg5 inhibitor monastrol (Figure 1A), whose binding site has been recently identified by X-ray crystallography (*27*). Then we applied this approach to study the binding of *S*-trityl-L-cysteine (Figure 1B), a potent inhibitor with antimitotic and tumoral growth inhibition activity (*28*) previously identified in our laboratory to inhibit Eg5 (*29*). This compound is ~40 times more effective *in vitro* and in cell-based assays than monastrol and thus can be considered as a potential anticancer agent.

EXPERIMENTAL PROCEDURES

Materials. Restriction enzymes were obtained from New England Biolabs. The QuickChange Site Directed Mutagenesis Kit was from Stratagene. Competent XL-10 and BL21-(DE3) pLysS cells were obtained from Novagen. The HighTrap chromatographic column was purchased from Amersham Pharmacia Biotech. TFA, PIPES, ATP, D_2O, lysozyme, pepsin, and kanamycin were all obtained from Sigma-Aldrich. IPTG was purchased from ICN. Acetonitrile (CH_3CN) was obtained from SDS. Racemic monastrol was purchased from BIOMOL Feinchemikalien. Chemicals for Eg5 ATPase assays were from sources indicated by Hackney and Jiang (*30*).

Pepsin Digestions. All protein digestions were performed in an ice bath at 0 °C. A pepsin solution (2.1 μg/μL) was prepared in 0.1 M H_3PO_4 (pH 1.6) and precooled to 0 °C using an ice bath. Eg5 constructs were digested for 2 min at pH 2.2 in 1 mM PIPES buffer with a protease/substrate ratio of 1/1 (w/w).

Sequence Assignments. The peptide fragments of nondeuterated Eg5 constructs were separated on a reverse phase C18 Interchrom column (1 mm × 100 mm) by using a linear gradient from 5 to 60% CH_3CN/H_2O (9/1, v/v) with 0.03% TFA (solvent B) over a run time of 60 min at a flow rate of 50 μL/min. Prior to the injection, the column was equilibrated with 95% solvent A (water with 0.03% TFA) and 5% solvent B for 20 min. Peptide assignments were performed by direct MS−MS analysis.

Preparation of Eg5−Inhibitor Complexes. Both monastrol and *S*-trityl-L-cysteine solutions (50 mM in DMSO) were diluted in 1 mM PIPES buffer (pH 7.3). The protein−inhibitor complexes were formed by using three different Eg5/inhibitor molar ratios (1/4, 1/13, and 1/20). The mixtures were incubated for 1 min at room temperature to allow complex formation.

Kinetics of H/D Exchange. Eg5 constructs (244 pmol) with or without inhibitor were diluted 25-fold in 1 mM deuterated PIPES buffer (pD 7.3) and incubated for several minutes at 0 °C. Isotopic back-exchange was quenched by addition of a precooled 0.1 M H_3PO_4 solution (pH 1.6) to decrease the pD of the mixture from 7.3 to 2.2. Samples were loaded on a C4 Protein MacroTrap cartridge (Michrom) and desalted with H_2O supplemented with 0.1% TFA. To limit isotopic back-exchange during the analysis, the column was precooled and maintained at 0 °C in an ice bath. Proteins were eluted with 60% CH_3CN/H_2O (9/1, v/v) with 0.1% TFA and analyzed by ESI-MS.

The percentage of incorporated deuterium (%D) was calculated by using eq 1

$$\%D = [(m_{x\%} - m)/(m_{100\%} - m)] \times 100 \qquad (1)$$

where m, $m_{x\%}$, and $m_{100\%}$ represent the average molecular mass of the protein obtained by analysis of nondeuterated, partially deuterated, and fully deuterated samples, respectively. $m_{100\%}$ was estimated from the amino acid sequence

[1] Abbreviations: ACES, *N*-(2-acetamido)-2-aminoethanesulfonic acid; DMSO, dimethyl sulfoxide; EDTA, ethylenediaminetetraacetic acid; EGTA, ethylene glycol bis(β-aminoethyl ether)-*N*,*N*,*N*′,*N*′-tetraacetic acid; H/D, hydrogen−deuterium; IPTG, isopropyl β-D-thiogalactopyranoside; ESI, electrospray ionization; LC−MS, liquid chromatography−mass spectrometry; MS, mass spectrometry; MS−MS, tandem mass spectrometry; PIPES, piperazine-*N*,*N*′-bis(2-ethanesulfonic acid); PMSF, phenylmethanesulfonyl fluoride; SDS−PAGE, sodium dodecyl sulfate−polyacrylamide gel electrophoresis; TFA, trifluoroacetic acid.

of the protein (number of exchangeable peptide amide hydrogens except proline residues). For Eg5 constructs, the maximum number of exchangeable amide hydrogens was calculated to be 380.

H/D Exchange Experiments of Peptide Fragments. Eg5 constructs (290 pmol) in the presence or absence of inhibitor were diluted 50-fold in deuterated buffer [1 mM PIPES (pD 7.3)]. Deuteration was performed at 0 °C for 5 min to exchange all accessible amide hydrogens of the protein with deuterium. Isotopic back-exchange was quenched by the addition of 6 μL of a precooled pepsin solution (pH 1.6). After pepsin digestion, deuterated peptide fragments were rapidly concentrated and desalted on a C4 Peptide MacroTrap cartridge (Michrom) at a flow rate of 300 μL/min. Deuterated peptides were separated on a reverse phase C18 Interchrom column (1 mm × 100 mm) by using a linear gradient from 5 to 100% CH_3CN/H_2O (9/1, v/v) with 0.03% TFA over a run time of 35 min at a flow rate of 50 μL/min. To limit isotopic back-exchanges, the column was precooled in an ice bath and maintained at 0 °C. The deuterated peptides were analyzed by ESI-MS.

ESI-MS and ESI-MS−MS Analysis. Kinetics of H/D exchange were determined on an API III+ triple-quadripole mass spectrometer equipped with an ionspray source (PE Sciex). The electrospray probe tip was held at 5 kV, and the declustering voltage was set at 80 V. Data were processed using Masspec 3.3 software, and the reconstructed molecular mass profiles were obtained by using a deconvolution algorithm from the *m*/*z* mass spectrum containing multiple charge states.

Sequence assignment and H/D exchange experiments on peptide fragments were performed on an ESQUIRE 3000+ quadripole ion trap mass spectrometer (Bruker Daltonics) equipped with an ionspray source. MS and MS−MS experiments were carried out with a capillary voltage set at 4 kV and an end plate offset voltage at 500 V. The gas nebulizer (N_2) pressure was set at 10 psi and the dry gas flow (N_2) at 8 L/min at a temperature of 250 °C. Mass spectra were analyzed using DataAnalysis 3.0 and Biotools 2.1.

Mass spectra of Eg5 proteins were obtained on a Q-TOF Micro mass spectrometer (Waters) equipped with a Z-spray ion source operating with a needle voltage of 3 kV. Sample Cone and Extraction Cone voltages were 30 and 4 V, respectively. Prior to analysis, samples were desalted on a C4 Protein MacroTrap cartridge (Michrom) with H_2O supplemented with 0.1% TFA. Proteins were eluted with 60% CH_3CN/H_2O (9/1, v/v) with 0.1% TFA and collected. Samples were then infused continuously at a flow rate of 7 μL/min, and the mass spectra were recorded in the range of *m*/*z* 500−2000. Spectra were acquired and processed with MassLynx 4.0.

Cloning of the Eg5 Mutant. The construction of Eg5 expression plasmid $pEg5_{1-386}$ used for mutagenesis experiments (encoding residues 1−386 of the motor domain and named Eg5) has been described recently (*13*). Two unique restriction sites (*Pml*I and *Bst*BI) were introduced by silent mutagenesis upstream and downstream of the $pEg5_{1-386}$ plasmid in the region encoding the potential monastrol binding sites identified by H/D exchange and mass spectrometry using DNA Strider (*31*). The following forward and reverse primers were used for the *Pml*I restriction site (position 5445): 5′-AAT GAA GAG TAC ACG TGG GAA GAG GAT CCC-3′ and 5′-GGG ATC CTC TTC CCA CGT GTA CTC TTC ATT-3′. The following were used for the *Bst*BI restriction site (position 5500): 5′-CCA CGT ACC CTT CAT CAA ATT TTC GAA AAA CTT ACT GAT-3′ and 5′-ATC AGT AAG TTT TTC GAA AAT TTG ATG AAG GGT ACG TGG-3′. The PCR was performed on the entire expression plasmid to produce daughter plasmids with the desired mutation, and the parental template was digested with *Dpn*I. After transformation into competent XL-10 cells, the resulting clones were tested on an agarose gel for the presence of *Pml*I and *Bst*BI restriction sites.

The two new restriction sites inserted into $pEg5_{1-386}$ delimit the main domain to be modified within the Eg5 motor domain. This domain was replaced by the equivalent nucleic acid sequences encoding residues 101−121 of *Neurospora crassa* conventional kinesin by restricting the expression plasmid with *Pml*I and *Bst*BI and inserting the following forward and reverse primers: 5′-G ATA GAT GAC CCT GAT GGC AGA GGT GTT ATT CCA AGA ATC GTC GAG CAA ATC TT-3′ and 5′-C GAA GAT TTG CTC GAC GAT TCT TGG AAT AAC ACC TCT GCC ATC AGG GTC ATC TAT C-3′. After ligation and transformation, the resulting clones were tested for the presence of the expected insert using the *Pml*I restriction enzyme. The *Pml*I restriction site is lost by insertion of the *N. crassa* sequence. The correctness of the cloning strategy was confirmed by DNA sequencing.

Expression and Purification of Recombinant Eg5 and Eg5-Nc Constructs. Eg5 was expressed and purified as described recently (*13*). The pEg5 expression construct containing the *N. crassa* kinesin heavy chain insertion (named Eg5-Nc) was transformed into competent BL21(DE3) pLysS *Escherichia coli* host cells for protein expression. Cells were grown overnight at 37 °C in a 500 mL flask supplemented with kanamycin (50 μg/mL); 150 mL was transferred into 3 L of 2×YT medium containing 50 μg/mL kanamycin, and cells were grown at 37 °C until an OD_{600} between 1.0 and 1.3 was reached. Recombinant Eg5 protein expression was induced by adding 0.5 mM IPTG to the cell culture. Cells were grown at room temperature for 20−24 h, harvested by centrifugation, frozen in liquid nitrogen, and stored at −80 °C.

The following steps were performed at 4 °C. The cells were resuspended in 60 mL of buffer A [20 mM PIPES (pH 7.3), 200 mM NaCl, 1 mM $MgCl_2$, and 1 mM EGTA] supplemented with 1 mM PMSF and 1 mg/mL lysozyme. The resuspended cells were incubated for 40 min and disrupted by three rapid freezing and defreezing cycles using liquid nitrogen. The solution was then incubated with 7 mM $MgCl_2$, 0.5 mM ATP, and 40 μL of DNase I (20 mg/mL) for 30 min and centrifuged for 40 min at 18 000 rpm and 4 °C (Beckmann JA20 rotor).

Purification was performed on an ÄKTA FPLC system equipped with a Frac-950 collector system (Amersham Bioscience). The supernatant was loaded onto a 5 mL Ni-charged HiTrap column previously equilibrated with buffer A. Bound Eg5 protein was eluted by using a step gradient of imidazole at a flow rate of 1 mL/min. Fractions (1 mL) were collected. Column fractions containing the recombinant protein were analyzed by SDS−PAGE, N-terminal sequencing, and mass spectrometry. The protein concentration of each fraction was estimated using the Bradford reagent (*32*).

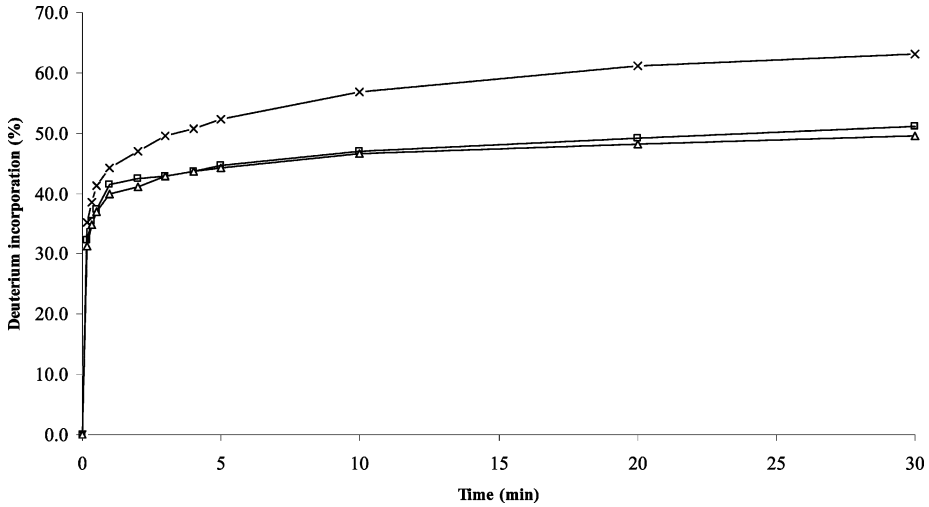

FIGURE 2: Deuterium incorporation time courses for the Eg5 motor domain alone (×) and in the presence of either a 4-fold molar excess of monastrol (□) or *S*-trityl-L-cysteine (△). These experiments were carried out in 1 mM deuterated PIPES (pD 7.3). Eg5 and Eg5−inhibitor complexes were incubated for several minutes at 0 °C. Isotopic back-exchange was quenched by decreasing the pD of each sample from 7.3 to 2.2.

The most concentrated fractions were aliquoted, frozen in liquid nitrogen, and stored at −80 °C.

Measurement of Basal ATPase Steady-State Kinetics. All experiments were performed at room temperature. Basal ATPase activities were measured using the pyruvate kinase/lactate dehydrogenase coupled assay in buffer A25A [25 mM ACES/KOH (pH 6.9), 2 mM magnesium acetate, 2 mM potassium EGTA, 0.1 mM potassium EDTA, and 1 mM β-mercaptoethanol] (*30*). The protein concentrations were 2.6 μM for Eg5 and 3.2 μM for Eg5-Nc. Activity was measured in the presence of various amounts of NaCl (up to 800 mM) or in the presence of monastrol or *S*-trityl-L-cysteine. For optimal inhibitor solubility, the assays were carried out in the presence of up to 2.2% DMSO. The data were analyzed using Kaleidagraph 3.0 (Synergy Software).

RESULTS

All H/D exchange experiments presented here were initiated by diluting the Eg5 motor domain in 1 mM deuterated PIPES buffer (pD 7.3). The protein was incubated in an ice bath, and the isotopic exchange reaction was quenched by decreasing the pD to 2.2. Samples were then subjected to either MS analysis or pepsin digestion followed by LC−MS analysis. On-line desalting as well as HPLC separation of deuterated samples was carried out with nondeuterated solvents so that all deuteriums located on the side chains and on the N- and C-termini of proteins or peptides are completely back-exchanged to hydrogen since the H/D exchange rates at these positions are several orders of magnitude faster than those of peptide amide linkages (*17*, *33*). As a result, the observed increase in the molecular weight of samples is due only to the incorporation of deuterium at peptide amide positions.

Global Hydrogen−Deuterium Exchange Studies. The H/D exchange behavior for the Eg5 motor domain alone and in the presence of a 4-fold molar excess of monastrol or of *S*-trityl-L-cysteine is shown in Figure 2. After 5 min, the extent of deuterium incorporation in Eg5 is ∼52%, corresponding to an exchange of ∼200 amide hydrogens of a possible 380. Subsequently, the deuterium incorporation rate is much slower. After 30 min, the percentage of deuterium incorporated reaches a value of ∼62%. A comparable percentage was obtained after deuteration for 120 min (data not shown), suggesting that most accessible amide hydrogens located on the surface of the Eg5 motor domain were exchanged during the first 5 min.

The presence of monastrol reduces the deuterium incorporation rate of the Eg5 motor domain (Figure 2). After 5 min, the extent of deuterium incorporation is 45%. Interestingly, a similar result was observed for *S*-trityl-L-cysteine with a level of deuterium incorporation of 44%. As shown in Figure 2, the kinetic curves obtained in the presence of the two inhibitors can be superimposed. Binding of these inhibitors reduces the amount of incorporation of deuterium into the Eg5 motor domain by ∼8%, corresponding to a solvent accessibility reduction of ∼30 backbone amide hydrogens. This decrease obtained after deuteration for 5 min was estimated to be sufficient for monitoring the effects of inhibitor binding on the deuterium exchange rate in peptide fragments.

Hydrogen−Deuterium Exchange Studies of Eg5 Peptide Fragments. The peptides obtained after pepsin digestion of the Eg5 motor domain for 2 min were identified by LC−ESI-MS−MS. Pepsin was used to digest the protein because this protease is active under conditions required for slowing amide hydrogen exchange (pH 2−3, 0 °C). Ninety-one proteolytic fragments were assigned, leading to a sequence coverage of the entire motor domain (Figure 3). The experiment was repeated after deuteration for 5 min by LC−ESI-MS to estimate the deuterium content of each peptide fragment identified and using HPLC conditions optimized for speed to minimize isotopic back-exchange. Under these conditions, deuteration can lead to overlapping mass peaks for coeluting peptides. Furthermore, the signals for deuterated peptides are in general lower than those of the corresponding nondeuterated peptides, due to nonhomogeneous deuteration which creates several species for a given peptide. As a result, the signal for some deuterated peptides may be lower than the noise level. After analysis, 59 deuterated peptide fragments were found, allowing 86% of the Eg5 motor domain to be covered (Figure 3). The following fragments were not recovered and are mainly located in the core region: residues

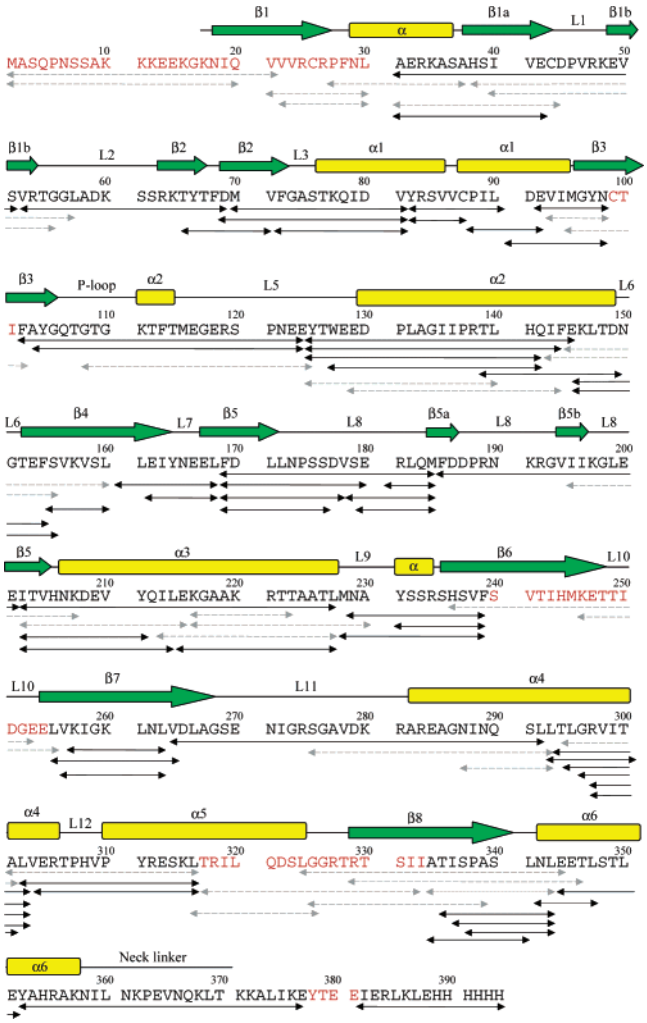

FIGURE 3: Protein sequence of the Eg5 motor domain showing the 91 pepsin-cleaved fragments identified by LC−ESI-MS−MS. Arrows below the sequence denote the position of each assigned proteolytic fragment. The 32 peptic fragments which were not recovered after deuteration for 5 min are denoted with dashed arrows, and their corresponding amino acid sequences are colored red. Secondary structural elements identified by X-ray crystallography (*34*) are shown above the sequence.

Asn18−Leu30 (β1), residues Ser240−Glu254 (β6 and loop 10), and residues Thr317−Ile333 (α5 and part of β8).

H/D exchange was then studied in the presence of a 4-fold molar excess of monastrol or *S*-trityl-L-cysteine. Monastrol binding reduces the extent of deuterium incorporation in eight peptide fragments from two regions within the Eg5 motor domain: Tyr125−Glu145 and Ile202−Leu227. The other 51 peptide fragments show no difference in deuterium incorporation. Results obtained for peptide fragments Tyr125−Glu145 and Ile202−Leu227 are shown in the mass spectra in Figure 4A. Structurally, the Tyr125−Glu145 fragment includes part of loop L5 and helix α2, and the Ile202−Leu227 fragment covers strand β5 and helix α3 (Figure 5A). Moreover, for the Eg5−*S*-trityl-L-cysteine complex, the deuterium incorporation rate of the same two peptides is modified, and it is notable that the variations observed in the mass spectra are similar for both inhibitors (Figure 4A). The H/D exchange experiment on Eg5 peptide fragments was also carried out in the presence of 13- and 20-fold molar excesses of inhibitors (data not shown). The results were the same as for a 4-fold molar excess, suggesting that no additional nonspecific binding to Eg5 occurs for these two molecules.

Characterization of Eg5 and Mutated Eg5-Nc Constructs. The recombinant Eg5-Nc protein was used to confirm the results obtained by H/D exchange in the presence of inhibitors. The Tyr125−Glu145 region of the Eg5 motor domain was replaced with the equivalent region in the *N. crassa* conventional kinesin heavy chain (NcKHC) (Figure 6). We chose NcKHC because this kinesin is not inhibited by monastrol and shares structural similarities with Eg5 (*13*, *34*). The modification of this region is expected to change the molecular mass of the Eg5 motor domain by 96 Da. The measured molecular masses of Eg5 and mutated Eg5-Nc proteins are 44 128 ± 2 and 44 030 ± 2 Da, respectively (data not shown). The experimental mass difference is 98 Da, very close to the theoretical value, confirming that the Tyr125−Glu145 region of the Eg5 protein was correctly replaced.

This result was also confirmed after pepsin digestion for 2 min at 0 °C followed by LC−ESI-MS analysis. The same peptide mapping was obtained for both Eg5 proteins. The only difference was found in the region modified within the mutated Eg5-Nc protein. Despite the inserted modification, the length of this peptide (Tyr125−Glu145 fragment) was not changed after pepsin digestion, allowing the molecular mass of the two peptide fragments to be compared. The measured molecular masses of the Tyr125−Glu145 fragment were 2398.4 and 2302.4 Da for Eg5 and mutated Eg5-Nc proteins, respectively (data not shown). This 96 Da mass difference clearly indicates that the mutated Eg5-Nc protein contains the NcKHC insert.

Basal ATPase Activity. The basal ATPase activities of Eg5 and mutated Eg5-Nc proteins were compared to check the activity of the mutated protein. The assays were carried out at various NaCl concentrations (up to 800 mM). The ATPase activity for both proteins increases with increasing amounts of NaCl, up to 350 mM. At higher salt concentrations, the ATPase activity decreases (Figure 7A). Eg5-Nc shows an ~2-fold decrease in the ATPase activity with a maximum velocity (V_{max}) of 0.055 s^{-1} compared to a value of 0.087 s^{-1} for Eg5. The basal ATPase activity was sufficiently conserved to allow the effects of inhibitors on the mutated protein to be monitored.

Measurement of the ATPase Activity in the Presence of Variable Amounts of Inhibitors. The IC_{50} values (median inhibitory concentration) were determined by measuring the basal ATPase activity of both Eg5 and Eg5-Nc proteins in the presence of increasing monastrol or *S*-trityl-L-cysteine concentrations. As illustrated in panels B and C Figure 7, both monastrol and *S*-trityl-L-cysteine inhibit the basal ATPase activity of the Eg5 protein. The IC_{50} values for the inhibition of Eg5 by monastrol and *S*-trityl-L-cysteine are 9.1 and 1.0 μM, respectively. In contrast, these two inhibitors have no effect on the mutated Eg5-Nc protein. The basal ATPase activity remains unaffected by increasing amounts of both inhibitors (Figure 7B,C), confirming that the Tyr125−Glu145 region is essential for binding both monastrol and *S*-trityl-L-cysteine.

Hydrogen/Deuterium Exchange Studies of Eg5-Nc Peptide Fragments. The studies of H/D exchange on Eg5-Nc peptide fragments were carried out in the presence of a 4-fold molar excess of monastrol or *S*-trityl-L-cysteine. After deuteration

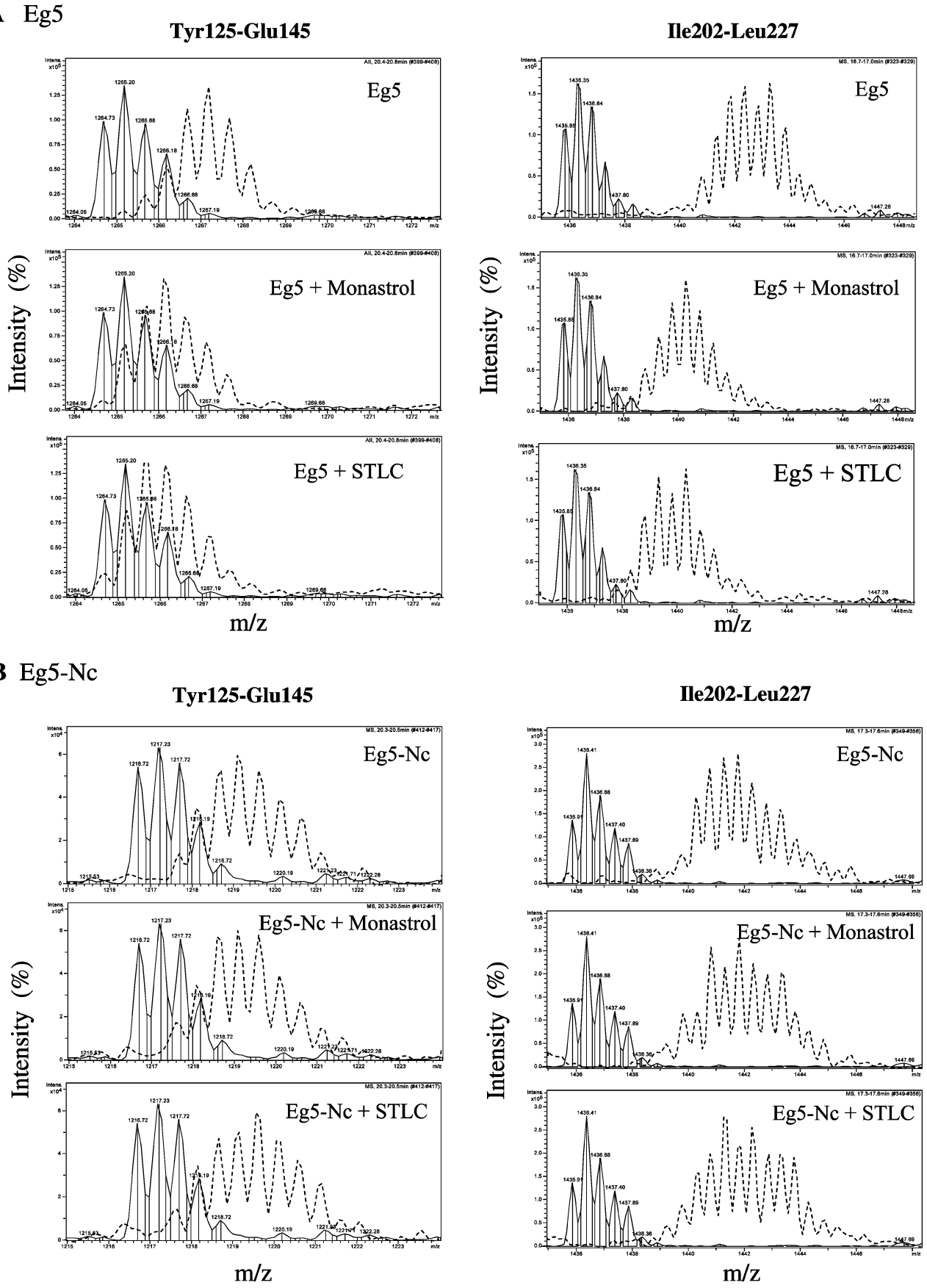

FIGURE 4: Effect of binding of monastrol and *S*-trityl-L-cysteine (STLC) on the deuterium level of the Tyr125−Glu145 and Ile202−Leu227 peptide fragments of (A) Eg5 and (B) Eg5-Nc. The formation of both Eg5−inhibitor complexes decreases the extent of deuterium incorporation by changing the solvent accessibility. No variation of deuterium incorporation is observed within the mutated Eg5-Nc protein in the presence of both inhibitors. Each mass spectrum compares the nondeuterated peptide fragment (—) with the peptide fragment without the inhibitor (- - -), in the presence of monastrol and in the presence of *S*-trityl-L-cysteine after deuteration for 5 min, respectively.

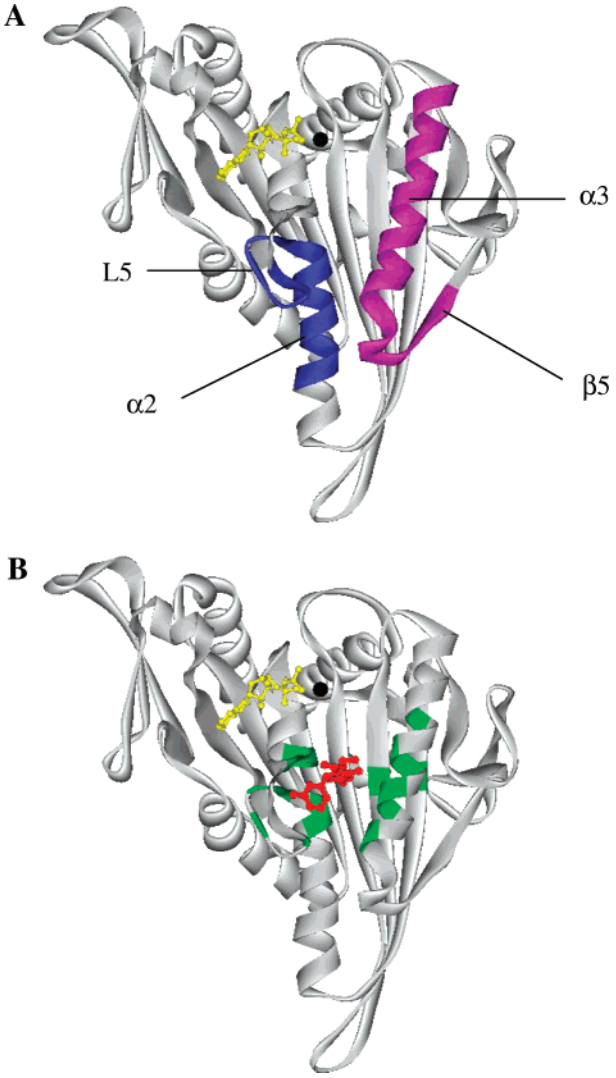

FIGURE 5: Ribbon representations of the Eg5 motor domain showing the inhibitor binding regions identified with our approach (A) and the monastrol binding site obtained by the recent structure determination of the ternary monastrol−ADP−Eg5 complex (B) by Yan *et al*. (*27*). MgADP is represented as a ball-and-stick model (yellow and black). (A) Regions identified by H/D experiments on peptic fragments in the presence of a 4-fold molar excess of inhibitors. Binding of monastrol or *S*-trityl-L-cysteine reduces the amount of deuterium incorporated into the same two regions. The first domain (colored blue) is composed of part of loop L5 and helix α2 (Tyr125−Glu145 peptic fragment); the second one (colored purple) comprises part of strand *β*5 and helix α3 (Ile202−Leu227 peptic fragment). (B) Monastrol binding site identified by X-ray crystallography. Binding of monastrol occurs in an induced fit pocket located between loop L5 and helix α3. The residues involved in monastrol binding are colored green. Monastrol (colored red) is represented as a ball-and-stick model. The figures were prepared using ViewerLite50.

and pepsin digestion, the same 59 peptide fragments that were obtained for the Eg5 motor domain (Figure 3) were found by LC−ESI-MS, allowing us to cover 86% of the Eg5-Nc sequence. The global fold of native and mutated Eg5 was compared by using H/D exchange−MS analysis. After incubation for 5 min, the deuteration pattern of the Eg5-Nc peptide fragments shows no significant difference compared to those of Eg5 fragments (data not shown). This means that the solvent accessibility is comparable for both proteins, indicating that the *N. crassa* insert does not induce dramatic changes in the structure of the mutated Eg5-Nc protein.

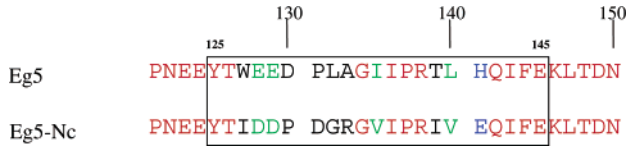

FIGURE 6: Comparison of the deleted Eg5 sequence (Tyr125−Glu145) and the inserted NcKHC sequence. Replacement of the Tyr125−Glu145 region (21 residues) with the equivalent NcKHC region modifies 11 amino acids in the mutated Eg5-Nc protein. Highly similar, weakly similar, and identical amino acids are colored green, blue, and red, respectively. Nonsimilar residues are colored black.

As shown in Figure 4B, the deuterium incorporation is unchanged within the modified Tyr125−Glu145 region of Eg5-Nc in the presence or absence of both inhibitors. The same result is obtained for the second identified potential inhibitor binding region (Ile202−Leu227, Figure 4B) as well as for the other 51 peptide fragments. Therefore, the presence of the NcKHC sequence prevents the solvent accessibility reduction induced by inhibitor binding within the Tyr125−Glu145 and Ile202−Leu227 regions.

DISCUSSION

We have identified the binding regions of small inhibitors targeting the human Eg5 motor domain using H/D exchange in association with protein digestion−mass spectrometry analysis (*16*, *17*) and directed mutagenesis. We tested the efficiency of our approach for determining the binding site of new Eg5 inhibitors using monastrol, a small cell permeable inhibitor of Eg5 activity, to compare our results with those obtained by X-ray crystallography of the ternary monastrol−ADP−Eg5 complex (*27*).

Monastrol binding decreases the H/D exchange rate of the Eg5 motor domain by ∼8% after deuteration for 5 min, corresponding to a reduction in the solvent accessibility of ∼30 backbone amide hydrogens. Because of the small size of monastrol (292 Da), the large overall decrease in the rate of H/D exchange observed here cannot be uniquely due to a masking effect. A possible explanation is that the interaction of monastrol with Eg5 leads to conformational changes within the protein. Two regions with reduced incorporation rates after formation of the Eg5−monastrol complex were identified using the protein digestion−MS method. The first region covers part of loop L5 and helix α2 (residues Tyr125−Glu145), and the second region is composed of strand *β*5 and helix α3 (residues Ile202−Leu227). To determine if the secondary structure elements identified were involved in monastrol binding, the region corresponding to residues Tyr125−Glu145 was replaced with the equivalent region from *N. crassa* conventional kinesin heavy chain (NcKHC). NcKHC is not inhibited by monastrol (*13*) despite being structurally similar to the human Eg5 motor domain. This implies that the small sequence differences in the conserved motor domain observed between NcKHC and human Eg5 are sufficient to explain the specificity of monastrol. The *N. crassa* protein sequence exchanged for the corresponding one in Eg5 is not expected to induce major changes in the structure of the mutated Eg5-Nc protein. The inserted NcKHC sequence modifies 11 residues, with five being highly similar and only six different (Figure 6), and the deuteration patterns of the Eg5-Nc peptide fragments are similar to those obtained for the Eg5 fragments. The main

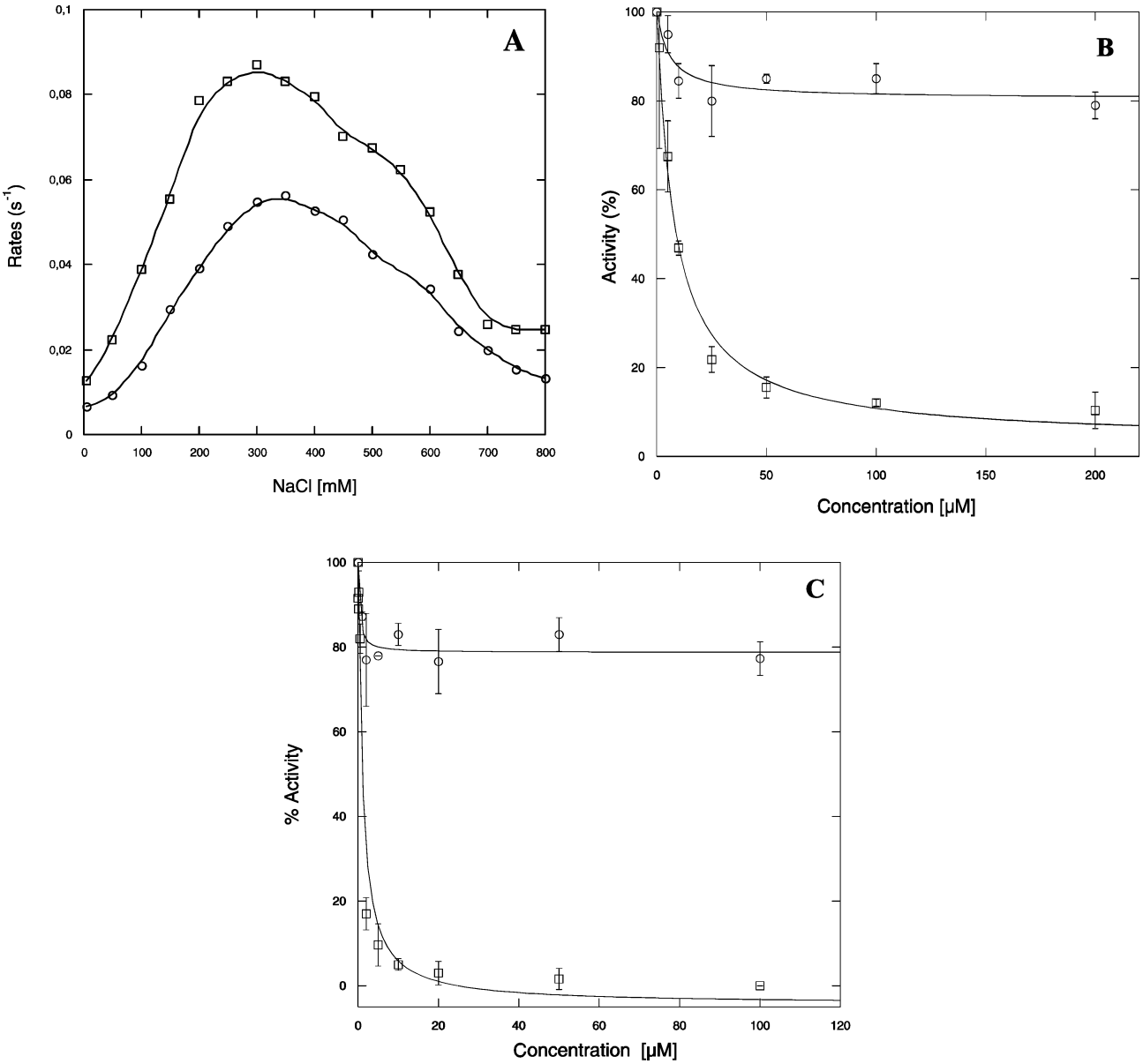

FIGURE 7: Measurement of the basal ATPase activity of Eg5 (□) and mutated Eg5-Nc (○) proteins. (A) Basal ATPase activity of Eg5 and Eg5-Nc in the presence of increasing NaCl concentrations. The insert of *N. crassa* induces an ~2-fold decrease in ATPase activity with V_{max} values of 0.087 and 0.055 s^{-1} for Eg5 and Eg5-Nc, respectively. (B and C) Inhibition of the basal ATPase activity of Eg5 and Eg5-Nc motor domains. (B) Monastrol inhibits the basal ATPase activity of the Eg5 motor domain with an IC_{50} value of 9.1 μM; no inhibition is observed with the mutated Eg5-Nc protein. (C) As for monastrol, formation of the Eg5−*S*-trityl-L-cysteine complex leads to the inhibition of the basal ATPase activity with an IC_{50} value of 1.0 μM. Again, no inhibition is observed for the mutated Eg5-Nc protein where the basal ATPase activity remains constant with increasing amounts of *S*-trityl-L-cysteine.

difference concerns loop L5. The length of this loop is variable among kinesin family members, and this loop is the longest in the human Eg5 motor domain (*35*) and should be slightly shorter in the Eg5-Nc protein. Despite this modification, the basal ATPase activity of the mutated Eg5-Nc was only 2-fold lower than that measured for Eg5 (Figure 7A). Monastrol does not inhibit the basal ATPase activity of mutated Eg5-Nc. The Tyr125−Glu145 region is thus directly implicated in monastrol binding.

We conclude that monastrol binding mainly involves loop L5 and helix α2 and that strand β5 and helix α3 should also be implicated. We are currently modifying the second region of the human Eg5 motor domain, but the results of the second mutation are not necessary for the conclusions presented here.

The results described above were compared to the recently published crystal structure of the ternary monastrol−ADP−Eg5 complex (*27*) (Figure 5). Binding of monastrol occurs in an induced fit pocket that is 12 Å from the ATP binding site of the protein. The inhibitor pocket is situated between helix α3 and loop L5. The creation of this pocket required local structural changes. The side chains of residues Arg119 (on helix α2), Trp127 (on loop L5), and Thr211 (on helix α3) are relocated to cap the entrance of the cavity and to accommodate space for the inhibitor. As a result, helix α3 shifts along its axis (by 1 Å), whereas helix α2 remains unaltered by the conformational modifications. The formation of this inhibitor pocket explains in part the ~8% solvent accessibility reduction which occurs when monastrol binds on the two regions identified by H/D exchange and mutational analysis (Figure 5A). There are 20 residues lining the monastrol pocket and surrounding the inhibitor for which the solvent accessibility may be altered in the ternary

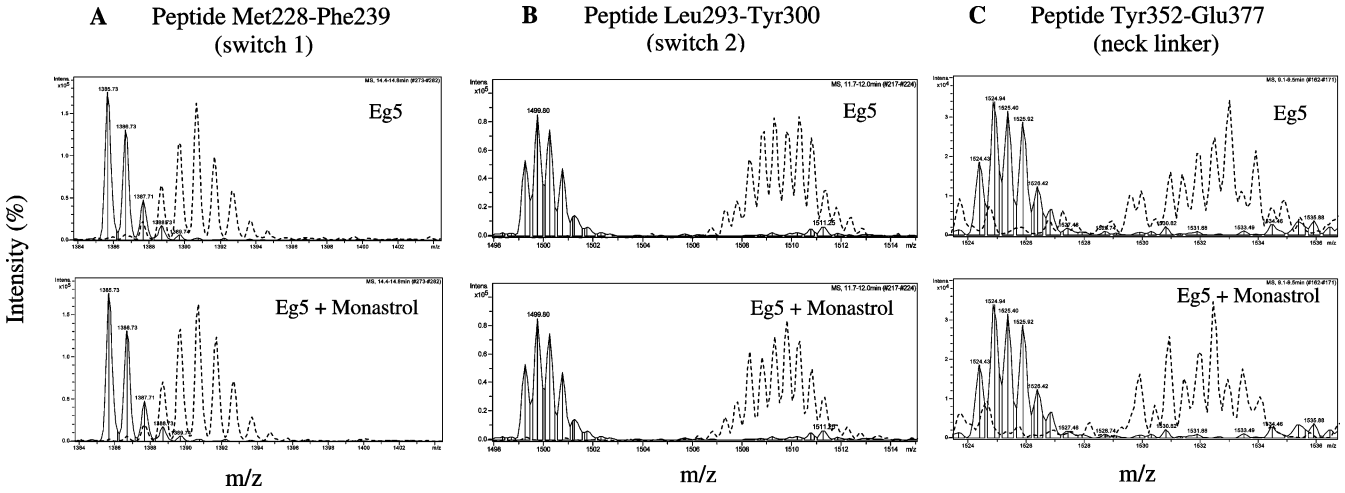

FIGURE 8: Effect of monastrol binding on the deuterium level of three peptide fragments: (A) Met228−Phe239 fragment (switch 1 region), (B) Ser264−Leu292 fragment (containing the switch 2 region), and (C) Tyr352−Glu377 fragment (neck linker). Each mass spectrum compares the nondeuterated peptide fragment (−) with the peptide fragment without the inhibitor, in the presence of monastrol and in the presence of *S*-trityl-L-cysteine after deuteration for 5 min, respectively.

complex due to both ligand protection and conformational changes (Figure 5B). In addition, Yan and colleagues (*27*) have shown that monastrol triggers distal structural changes throughout the Eg5 motor domain. These rearrangements take place within switch 1 (Asn229−Arg234), within switch 2 (Asp265−Glu270), and in the neck linker regions (Asn358−Pro363). Switch 1 is found at the end of helix α3 and consists of a loop in Eg5 (*35*). This loop becomes a short helix upon monastrol binding, leading to a shift of switch 1 of ∼6 Å. This modification was not identified with our method, although a change in the secondary structure of switch 1 should result in modification of the H/D exchange rate. The peptide fragment corresponding to switch 1 does not exhibit differences in the extent of deuterium incorporation after monastrol binding (Figure 8A). Similar results were obtained for switch 2 (Figure 8B). The deuteration time used (5 min) was sufficient to allow complete isotopic exchange within these two regions in the presence or absence of monastrol. The other conformational changes concern the neck linker. The structural changes triggered in this region upon monastrol binding are difficult to estimate with our method due to nonhomogeneous deuteration of the Tyr352−Glu377 peptide (Figure 8C).

With regard to monastrol, the formation of the Eg5−*S*-trityl-L-cysteine complex induces an ∼8% decrease in the deuteration rate after incubation for 5 min. Because of the size of this molecule (363 Da), the observed overall variation can only be due to both a masking effect and conformational changes within the motor domain. Interestingly, *S*-trityl-L-cysteine modifies the same two regions implicated in monastrol binding. This result is surprising because these two inhibitors vary considerably in their structure (Figure 1). In addition, the decrease in the extent of deuterium incorporation observed in the Tyr125−Glu145 and Ile202−Leu227 regions is similar for both inhibitors. This means that the solvent accessibility reduction concerns the same number of amide peptide linkages. Incubation of *S*-trityl-L-cysteine with the mutated Eg5-Nc does not affect the basal ATPase activity, whereas a strong inhibition is observed with Eg5. The Tyr125−Glu145 region is thus directly involved in *S*-trityl-L-cysteine binding since no inhibition occurs when this domain is modified. We conclude that *S*-trityl-L-cysteine binds to the same region in human Eg5 as monastrol. This raises the question of how these molecules inhibit Eg5 ATPase activity. We know that monastrol inhibits ADP release by forming a ternary complex (*12*, *13*), and residues Trp127, Asp130, Leu132, and Ala133 seem to play a major role since the basal Eg5 ATPase activity is no longer inhibited when we mutate these four amino acid residues in our Eg5construct to Ile, Pro, Gly, and Arg, respectively (Figure 6). It seems likely that replacing residue Trp127 with Ile prevents the formation of the induced fit pocket and thus the relocation of the side chains of Arg119 (on helix α2) and Tyr211 (on helix α3) which are known to accommodate space for the inhibitor. Hence, the local and distal structural changes throughout the motor domain do not occur, nor does formation of the ternary complex since no variation of deuterium incorporation is observed within the mutated Eg5-Nc protein in the presence of both inhibitors (Figure 4B).

The approach described here can thus be used to probe rapidly the interaction between other small molecules and Eg5. The combination of H/D exchange experiments with mass spectrometry and directed mutagenesis allows the regions within the protein involved in ligand binding and/or conformational changes to be pinpointed. This method will be useful for the rapid identification of other Eg5 inhibitor binding regions prior to X-ray structure determination, since once the peptide mapping is in hand, the identification of the interacting site for other Eg5 inhibitors only takes ∼1 week. However, one should always keep in mind that it is likely that ligand binding induces local conformational changes within the interaction site and major long distance changes to other sites throughout the protein (*36*). In this case, the discrimination between the masking effect and the conformational changes is difficult especially when the ligand is small. For the Eg5 motor domain, binding of both inhibitors triggers major structural changes within the interaction site. As a result, the variation of the monitored H/D exchange rate corresponds to both a masking effect and conformational changes.

The recent studies of the Eg5 mRNA expression pattern in normal human tissues by Sakowicz *et al.* (*15*) have demonstrated the interest in targeting this mitotic kinesin for the discovery of novel antimitotic cancer drugs. Eg5 appears

to be most abundant in proliferating tissues and absent in postmitotic human central nervous system neurons. These results, taken together, suggest that the inhibition of the Eg5 function will only occur in proliferating cells (including cancerous cells). We showed here that *S*-trityl-L-cysteine and monastrol bind to the same region on HsEg5 by induced fit in a pocket formed by helix α3−strand β5 and loop L5−helix α2. Both inhibitors trigger local conformational changes within the interaction site, and it seems likely that they share a similar mechanism for inhibition of Eg5−ATPase activity. *S*-Trityl-L-cysteine is ∼40 times more effective *in vitro* and in cell-based assays than monastrol and is able to induce mitotic arrest in HeLa cells without any visible effect on interphase cells (*29*). In conclusion, *S*-trityl-L-cysteine leads to tumor growth inhibition as shown, for example, in the NCI 60 tumor cell line screen (GI_{50} = 1.3 μM), and the identification of the binding region on Eg5 is a first step in understanding its mechanism of action.

ACKNOWLEDGMENT

We thank Jean-Pierre Andrieu for N-terminal sequencing of Eg5 constructs. We also thank the Drug Synthesis & Chemistry Branch, Developmental Therapeutics Program, Division of Cancer Treatment and Diagnosis, for providing us with *S*-trityl-L-cysteine. We thank Dr. Richard Wade (Institut de Biologie Structurale) and Dr. James Conway (Institut de Biologie Structurale) for helpful discussions.

REFERENCES

1. Wood, K. W., Cornwell, W. D., and Jackson, J. R. (2001) Past and future of the mitotic spindle as an oncology target, *Curr. Opin. Pharmacol. 1*, 370−377.
2. Rowinski, E. K., Chaudhry, V., Cornblath, D. R., and Donehower, R. C. (1993) Neurotoxicity of Taxol, *J. Natl. Cancer Inst. 15*, 107−115.
3. Cole, S. P., Sparks, K. E., Fraser, K., Loe, D. W., Grant, C. E., Wilson, G. M., and Deeley, R. G. (1994) Pharmacological characterization of multidrug resistant MRP-transfected human tumor cells, *Cancer Res. 54*, 5902−5910.
4. Walczak, C. E., and Mitchison, T. J. (1996) Kinesin-related proteins at mitotic spindle poles: function and regulation, *Cell 85*, 943−946.
5. Kashina, A. S., Rogers, G. C., and Scholey, J. M. (1997) The bimC family of kinesins: essential bipolar mitotic motors driving centrosome separation, *Biochim. Biophys. Acta 1357*, 257−271.
6. Blangy, A., Lane, H. A., d'Herin, P., Harper, M., Kress, M., and Nigg, E. A. (1995) Phosphorylation by $p34^{cdc2}$ regulates spindle association of human Eg5, a kinesin-related motor essential for bipolar spindle formation in vivo, *Cell 83*, 1159−1169.
7. Sawin, K. E., and Mitchison, T. J. (1995) Mutations in the kinesin-like protein Eg5 disrupting localization to the mitotic spindle, *Proc. Natl. Acad. Sci. U.S.A. 92*, 4289−4293.
8. Blangy, A., Arnaud, L., and Nigg, E. A. (1997) Phosphorylation by $p34^{cdc2}$ protein kinase regulates binding of the kinesin-related motor HsEg5 to the dynactin subunit p150, *J. Biol. Chem. 272*, 19418−19424.
9. Miyamoto, D. T., Perlman, Z. E., Mitchison, T. J., and Shirasu-Hiza, M. (2003) Dynamics of the mitotic spindle: potential therapeutic targets, *Prog. Cell Cycle Res. 5*, 349−360.
10. Mayer, T. U., Kapoor, T. M., Haggarty, S. J., King, R. W., Schreiber, S. L., and Mitchison, T. J. (1999) Small molecule inhibitor of mitotic spindle bipolarity identified in a phenotype-based screen, *Science 286*, 971−974.
11. Kapoor, T. M., Mayer, T. U., Coughlin, M. L., and Mitchison, T. J. (2000) Probing spindle assembly mechanisms with monastrol, a small molecule inhibitor of the mitotic kinesin, *J. Cell Biol. 150*, 975−988.
12. Maliga, Z., Kapoor, T. M., and Mitchison, T. J. (2002) Evidence that monastrol is an allosteric inhibitor of the mitotic kinesin Eg5, *Chem. Biol. 9*, 989−996.
13. DeBonis, S., Simorre, J. P., Crevel, I., Lebeau, L., Skoufias, D. A., Blangy, A., Ebel, C., Gans, P., Cross, R., Hackney, D. D., Wade, R. H., and Kozielski, F. (2003) Interaction of the mitotic inhibitor monastrol with human kinesin Eg5, *Biochemistry 42*, 338−349.
14. Nakazawa, J., Yajima, J., Usui, T., Ueki, M., Takatsuki, A., Imoto, M., Toyoshima, Y. Y., and Osada, H. (2003) A novel action of terpendole E on the motor activity of mitotic kinesin Eg5, *Chem. Biol. 10*, 131−137.
15. Sakowicz, R., Finer, J. T., Beraud, C., Crompton, A., Lewis, E., Fritsch, A., Lee, Y., Mak, J., Moody, R., Turincio, R., Chabala, J. C., Gonzales, P., Roth, S., Weitman, S., and Wood, K. W. (2004) Antitumor activity of a kinesin inhibitor, *Cancer Res. 64*, 3276−3280.
16. Englander, J. J., Rogero, J. R., and Englander, S. W. (1985) Protein hydrogen exchange studied by the fragment separation method, *Anal. Biochem. 147*, 234−244.
17. Zhang, Z., and Smith, D. L. (1993) Determination of amide hydrogen exchange by mass spectrometry: a new tool for protein structure elucidation, *Protein Sci. 2*, 522−531.
18. Smith, D. L., Deng, Y., and Zhang, Z. (1997) Probing the non-covalent structure of proteins by amide hydrogen exchange and mass spectrometry, *J. Mass Spectrom. 32*, 135−146.
19. Dharmasiri, K., and Smith, D. L. (1996) Mass spectrometric determination of isotopic exchange rates of amide hydrogens located on the surfaces of proteins, *Anal. Chem. 68*, 2340−2344.
20. Zhang, Z., Post, C. B., and Smith, D. L. (1996) Amide hydrogen exchange determined by mass spectrometry: application to rabbit muscle aldolase, *Biochemistry 35*, 779−791.
21. Wang, F., and Tang, X. (1996) Conformational heterogeneity of stability of apomyoglobin studied by hydrogen/deuterium exchange and electrospray ionization mass spectrometry, *Biochemistry 35*, 4069−4078.
22. Milne, J. S., and Mayne, L. (1998) Determinants of protein hydrogen exchange studied in equine cytochrome *c*, *Protein Sci. 7*, 739−745.
23. Mandell, J. G., Falick, A. M., and Komives, E. A. (1998) Identification of protein−protein interfaces by decreased amide proton solvent accessibility, *Proc. Natl. Acad. Sci. U.S.A. 95*, 14705−14710.
24. Ehring, H. (1999) Hydrogen exchange/electrospray ionization mass spectrometry studies of structural features of proteins and protein/protein interactions, *Anal. Biochem. 267*, 252−259.
25. Akashi, S., and Takio, K. (2000) Characterization of the interface structure of enzyme−inhibitor complex by using hydrogen−deuterium exchange and electrospray ionization Fourier transform ion cyclotron resonance mass spectrometry, *Protein Sci. 9*, 2497−2505.
26. Gonzalez de Peredo, A., Saint-Pierre, C., Latour, J. M., Michaud-Soret, I., and Forest, E. (2001) Conformational changes of the ferric uptake regulation protein upon metal activation and DNA binding; first evidence of structural homologies with the diphtheria toxin repressor, *J. Mol. Biol. 310*, 83−91.
27. Yan, Y., Sardana, V., Xu, B., Homnick, C., Halczenko, W., Buser, C. A., Schaber, M., Hartman, G. D., Huber, H. E., and Kuo, L. C. (2004) Inhibition of a mitotic motor protein: where, how, and conformational consequences, *J. Mol. Biol. 335*, 547−554.
28. Paull, K. D., Lin, C. M., Malspeis, L., and Hamel, E. (1992) Identification of novel antimitotic agents at the tubulin level by computer-assisted evaluation of differential cytotoxicity data, *Cancer Res. 52*, 3892−3900.
29. DeBonis, S., Skoufias, D. A., Lebeau, L., Robin, G., Margolis, R., Wade, R. H., and Kozielski, F. (2004) In vitro screening for inhibitors of the human mitotic kinesin, Eg5, with antimitotic and antitumor activity, *Mol. Cancer Ther. 3*, 1079−1090.
30. Hackney, D. D., and Jiang, W. (2001) Assays for kinesin microtubule-stimulated ATPase activity, *Methods Mol. Biol. 164*, 65−71.
31. Marck, C. (1988) 'DNA Strider': a 'C' program for the fast analysis of DNA and protein sequences on the Apple Macintosh family of computers, *Nucleic Acids Res. 16*, 1829−1836.
32. Bradford, M. M. (1976) A rapid and sensitive method for the quantitation of microgram quantities of protein utilizing the principle of protein-dye binding, *Anal. Biochem. 72*, 248−254.

33. Thevenon-Emeric, G., Kozlowski, J., Zhang, Z., and Smith, D. L. (1992) Determination of amide hydrogen exchange rates in peptides by mass spectrometry, *Anal. Chem. 64*, 2456−2458.
34. Song, Y. H., Marx, A., Muller, J., Woehlke, G., Schliwa, M., Krebs, A., Hoenger, A., and Mandelkow, E. (2001) Structure of a fast kinesin: implications for ATPase mechanism and interactions with microtubules, *EMBO J. 20*, 6213−6225.
35. Turner, J., Anderson, R., Guo, J., Beraud, C., Fletterick, R., and Sakowicz, R. (2001) Crystal structure of the mitotic spindle kinesin Eg5 reveals a novel conformation of the neck-linker, *J. Biol. Chem. 276*, 25496−25502.
36. Anand, G. S., Hughes, C. A., Jones, J. M., Taylor, S. S., and Komives, E. A. (2002) Amide H/^{2}H exchange reveals communication between the cAMP and catalytic subunit-binding sites in the R(I)α subunit of protein kinase A, *J. Mol. Biol. 323*, 377−386.

BI049264E